Partial spin-crossover behaviour in a dinuclear iron(II) triple helicate

Rosanna J. Archer,[a] Chris S. Hawes,[a] Guy N. L. Jameson,[b] Vickie McKee,[c] Boujemaa Moubaraki,[d] Nicholas F. Chilton,[d] Keith S. Murray,[d] Wolfgang Schmitt[e] and Paul E. Kruger*[a]

Electronic Supporting Information (ESI)

Table S1 Parameters of intra-molecular C-H···π interactions (Cg = centre of ring) within **1**(H_2O) and **1**(MeCN)**.**

C–H…Cg	C–H/Å	*d*(H…Cg)/Å	*d*(C…Cg)/Å	<(C-H…Cg)/°
1(H_2O)				
C7–H7A···Cg	0.95	2.58	3.48	157
C58–H58A···Cg	0.95	3.03	3.86	147
1(MeCN)				
C30–H30···Cg	0.93	2.57	3.47	157
C59–H59···Cg	0.93	2.67	3.59	170

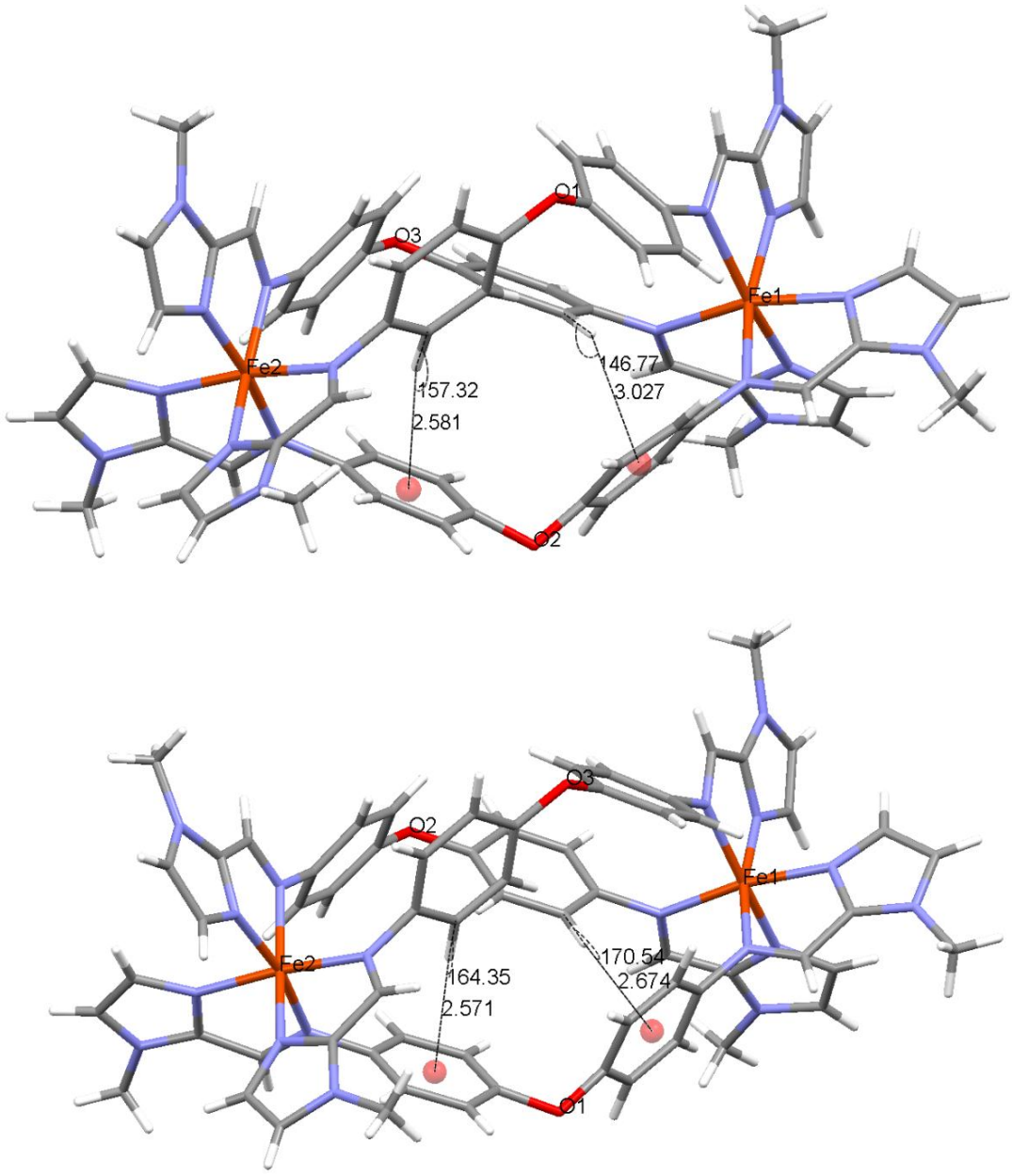

Figure S1: The intra-molecular C-H···π interactions within **1**(H_2O) (top) and **1**(MeCN) (bottom) showing the parameters associated with these interactions.

Figure S2: Comparison of the crystal packing for **1**(MeCN) and **1**(H_2O) to illustrate their similarities and differences**.** The 'ends' of the helicates that contain low spin Fe(II) are coloured blue whereas the 'ends' containing high spin Fe(II) are coloured orange; perchlorate anions are coloured green and the solvent molecules are coloured red. Hydrogen atoms omitted for clarity.

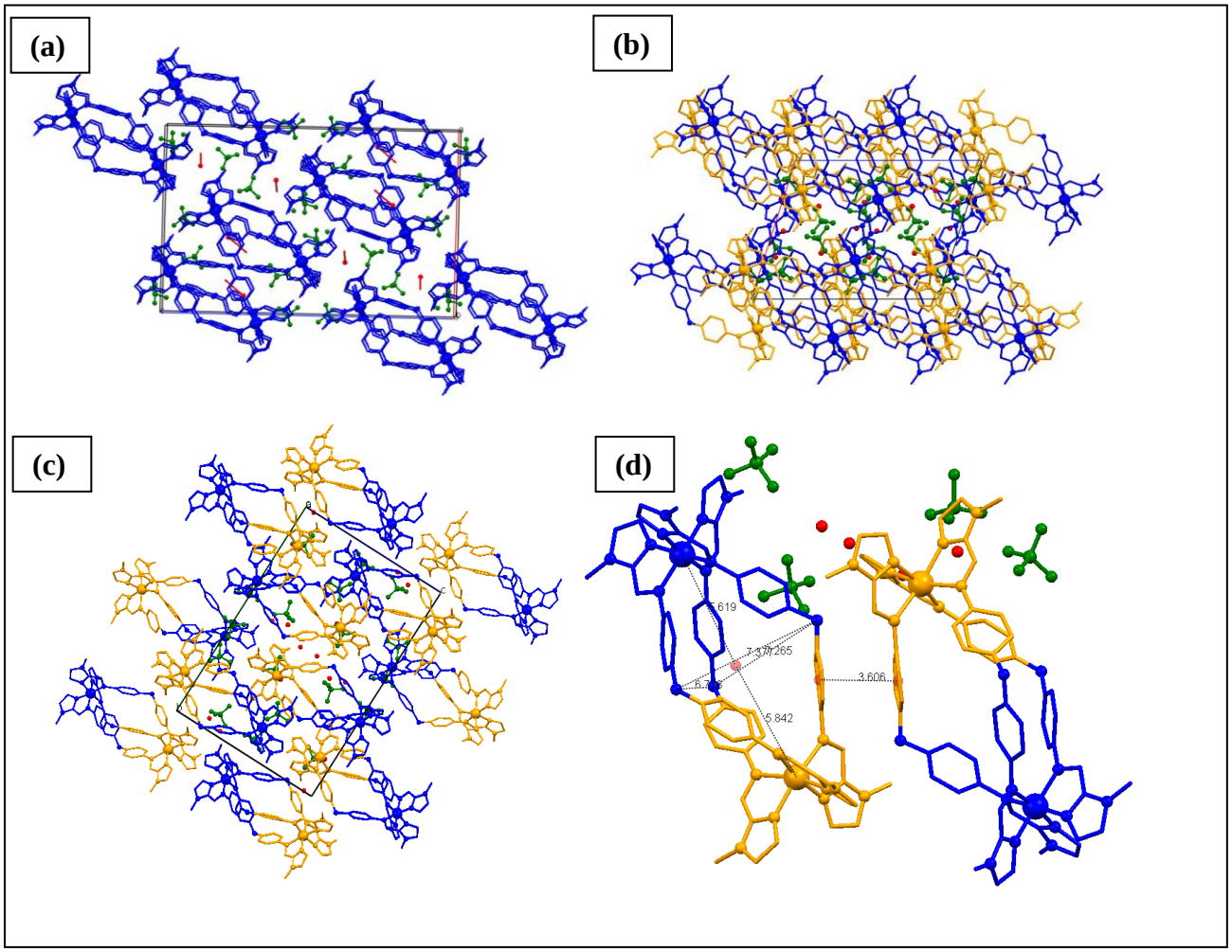

(**a**) **1**(MeCN) viewed down the crystallographic *b*-axis. Note how $[Fe_2L_3]^{4+}$ units pack in series down the *b*-axis.

(**b**) **1**(H_2O) viewed down the crystallographic *b*-axis. Note how $[Fe_2L_3]^{4+}$ units pack alternatively.

(**c**) **1**(H_2O) viewed so that the orientation best matches that of **1**(MeCN) shown in (**a**). Note the intermolecular face-to-face π···π interaction between adjacent helicates.

(**d**) Packing diagram for **1**(H_2O) showing a close-up of the intermolecular π-π-interactions between adjacent helicate species and pertinent intra-helical distances as dashed lines**.**

Thermogravimetric Analysis: The variable water content of **1**(H_2O) was analysed through careful TGA experiments. Because of the potential hazards due to the presence of perchlorate the samples were not heated above 100 °C.

The initial experiment was performed upon an air-dried sample of **1**(H_2O) that was heated at 1 °C/min to 100 °C and held at 100 °C for 120 minutes (lower blue trace in Fig. S3). It is clear that water loss occurs immediately from 20 °C. During the course of this experiment a total weight loss of *ca.* 4.08 % was noted which corresponds to the loss of four water molecules (calc. 4.15 %). This sample was then left overnight open to the air and a second experiment was conducted whereupon the sample was again heated at 1 °C/min to 100 °C and held at 100 °C for 120 minutes (upper green trace in Fig. S3). During this experiment a total weight loss of *ca.* 2.51 % was noted which corresponds to a loss of *ca.* 2.5 water molecules (calc. 2.64 %).

Furthermore, the TGA experiment performed upon the sample recovered from the magnetic susceptibility measurements, after being exposed to air for several weeks, also indicated that water re-absorption had occurred and a similar weight loss profile was obtained (not shown) accounting to a comparable loss of water molecules indicative of the pristine 'mother' sample. Indeed, visual inspection of the samples post-TGA measurements reveals that they retain their crystallinity.

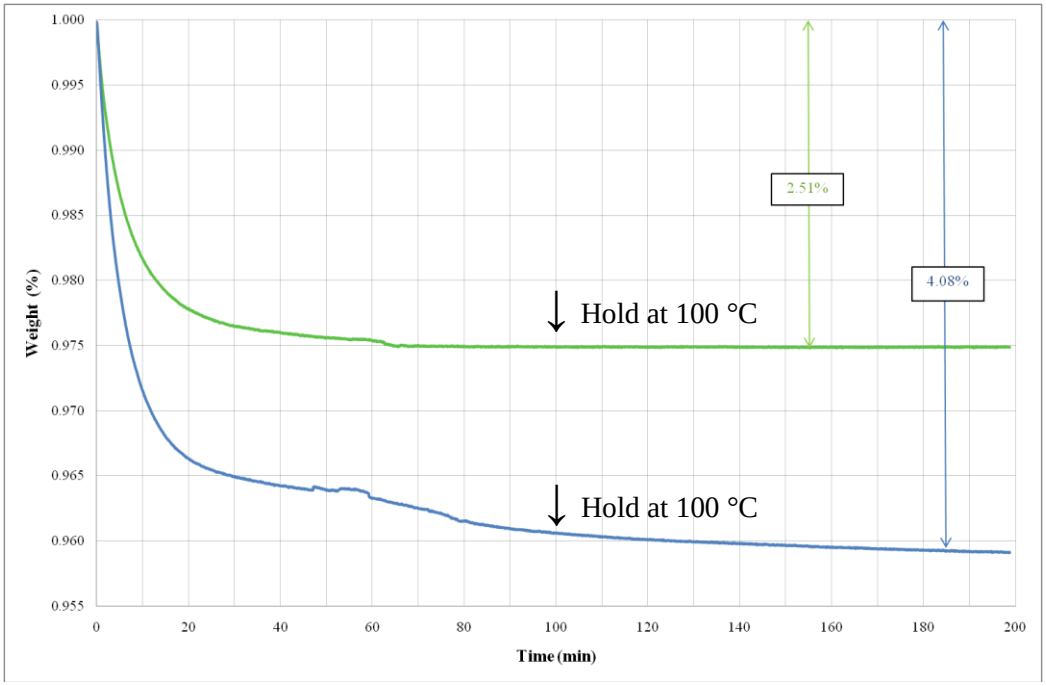

Figure S3: TGA for **1**(H_2O) showing the variable loss and re-absorption of water. The lower blue trace is that for the original air-dried sample whereas the upper green trace is for this sample post-TGA after it had been left open to the atmosphere over night to re-hydrate.

Figure S4: ES Mass Spectrum of **1**(H_2O) comparing the experimental isotope pattern (top) to the theoretical isotope pattern (bottom).

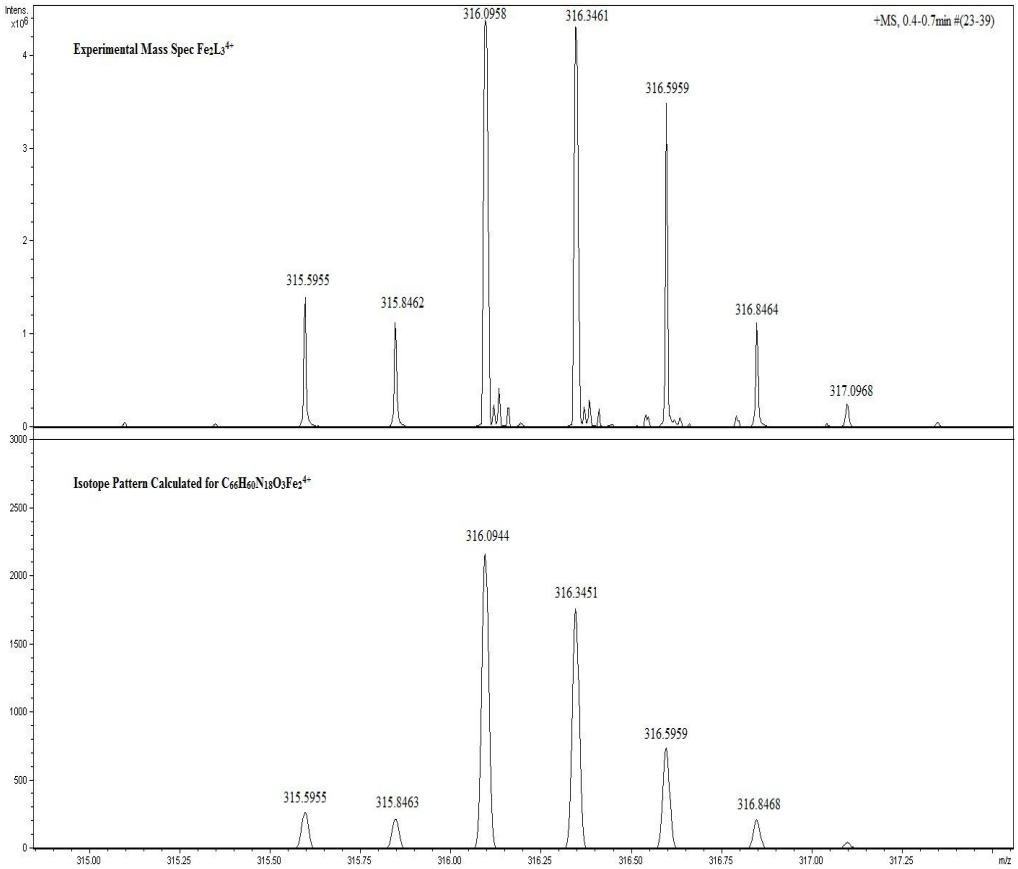

X-ray Diffraction: Single crystal data and experimental details for **1**(H_2O) are summarised in Table S2. The single crystal analysis was performed at 150(2) K on line 11.3.1 of the Advanced Light Source.

All of the crystals were very thin (curly!) laths, several were tried and each gave very broad, streaky, low intensity peaks but the same unit cell. The structure was solved by direct methods and refined on F^2. All the non-H atoms were refined anisotropically (using SIMU and DELU restraints) and H atoms were inserted at calculated positions except for those of the partial occupancy water molecules, which were not included in the model. Due to the very weak data, the statistics (R_{int} etc) are poor but, nevertheless the refinement behaved reasonably well. It converged at R1 = 12.4% for data out to $2\theta = 45°$, higher angle data were not used in the refinement as there was no significant intensity present. Unsurprisingly, checkcif produces a range of alerts for this structure; these are all due to the basic problem of the very weak data but, given that the data were collected on a synchrotron, there is no real prospect of an improved data set. However, the cell and structure are basically correct, the geometry and bond distances are all in the expected ranges and the differences between the two iron sites are clear-cut (see Table S3 below). Assignment of the solvate molecules as water is supported by the characterisation studies of the bulk sample and also by the observation that they make a reasonable (and finite) H-bonded unit with the perchlorate anions (Fig S5). O1w and O2w were refined with 50% occupancy, O3w and O4w with 25% occupancy. Partial loss of water molecules may be the cause of the broad diffraction peaks. Selected bond lengths [Å] and angles [°] for **1**(H_2O) are given in Table S3.

Table S2. Crystal data and structure refinement for **1**(H_2O).

Identification code	**1·H_2O**	
Empirical formula	$C_{66}H_{60}Cl_4Fe_2N_{18}O_{20.50}$	
Formula weight	1686.82	
Temperature	150(2) K	
Wavelength	0.77490 Å	
Crystal system	Monoclinic	
Space group	P2(1)/c	
Unit cell dimensions	a = 14.82(4) Å	α= 90°.
	b = 27.22(8) Å	β= 107.88(4)°.
	c = 18.98(6) Å	γ = 90°.
Volume	7284(36) $Å^3$	
Z	4	
Density (calculated)	1.538 Mg/m^3	
Absorption coefficient	0.632 mm^{-1}	
F(000)	3464	
Crystal size	0.41 x 0.11 x 0.01 mm^3	
Crystal description	orange thin plate	
Theta range for data collection	2.95 to 22.50°.	
Index ranges	-14<=h<=14, -26<=k<=26, -18<=l<=18	
Reflections collected	37303	
Independent reflections	7330 [R(int) = 0.5358]	
Completeness to theta = 22.50°	99.8 %	
Absorption correction	Semi-empirical from equivalents	
Max. and min. transmission	0.8621 and 0.4708	
Refinement method	Full-matrix least-squares on F^2	
Data / restraints / parameters	7330 / 1996 / 1019	
Goodness-of-fit on F^2	1.184	
Final R indices [I>2sigma(I)]	R1 = 0.1242, wR2 = 0.2600	
R indices (all data)	R1 = 0.3104, wR2 = 0.3435	
Extinction coefficient	0.0035(4)	
Largest diff. peak and hole	0.670 and -1.029 e.$Å^{-3}$	

Table S3. Selected bond lengths [Å] and angles [°] for **1**(H_2O).

Fe(1)-N(12)	2.116(14)	Fe(2)-N(13)	1.931(16)
Fe(1)-N(18)	2.130(16)	Fe(2)-N(1)	1.936(16)
Fe(1)-N(6)	2.132(17)	Fe(2)-N(7)	1.948(12)
Fe(1)-N(16)	2.168(14)	Fe(2)-N(3)	1.965(14)
Fe(1)-N(10)	2.255(17)	Fe(2)-N(15)	1.984(17)
Fe(1)-N(4)	2.287(16)	Fe(2)-N(9)	1.984(16)

N(12)-Fe(1)-N(18)	89.1(7)	N(13)-Fe(2)-N(1)	88.9(8)
N(12)-Fe(1)-N(6)	90.3(6)	N(13)-Fe(2)-N(7)	92.1(6)
N(18)-Fe(1)-N(6)	88.2(7)	N(1)-Fe(2)-N(7)	92.7(7)
N(12)-Fe(1)-N(16)	165.8(7)	N(13)-Fe(2)-N(3)	90.7(7)
N(18)-Fe(1)-N(16)	78.1(6)	N(1)-Fe(2)-N(3)	80.2(6)
N(6)-Fe(1)-N(16)	95.3(6)	N(7)-Fe(2)-N(3)	172.3(7)
N(12)-Fe(1)-N(10)	76.5(6)	N(13)-Fe(2)-N(15)	80.8(7)
N(18)-Fe(1)-N(10)	96.2(7)	N(1)-Fe(2)-N(15)	166.3(7)
N(6)-Fe(1)-N(10)	166.0(5)	N(7)-Fe(2)-N(15)	96.8(7)
N(16)-Fe(1)-N(10)	98.6(6)	N(3)-Fe(2)-N(15)	90.7(6)
N(12)-Fe(1)-N(4)	95.6(6)	N(13)-Fe(2)-N(9)	171.8(6)
N(18)-Fe(1)-N(4)	164.2(7)	N(1)-Fe(2)-N(9)	92.3(8)
N(6)-Fe(1)-N(4)	76.7(6)	N(7)-Fe(2)-N(9)	79.7(6)
N(16)-Fe(1)-N(4)	98.4(5)	N(3)-Fe(2)-N(9)	97.5(7)
N(10)-Fe(1)-N(4)	99.6(7)	N(15)-Fe(2)-N(9)	99.2(8)

C(12)-O(1)-C(9)	119.0(14)
C(34)-O(2)-C(31)	113.1(13)
C(56)-O(3)-C(53)	118.2(14)

Figure S5 Asymmetric unit of **1**(H_2O). The H-bonded chain does not extend further in any direction.

H-bond distances [Å]:

O1W - O22	2.781 (0.032)
O1W - O31	2.777 (0.036)
O2W - O11	2.666 (0.035)
O2W - O41	2.993 (0.030)
O3W - O4W	2.892 (0.059)
O3W - O32	3.015 (0.047)
O4W - O2W	2.927 (0.050)

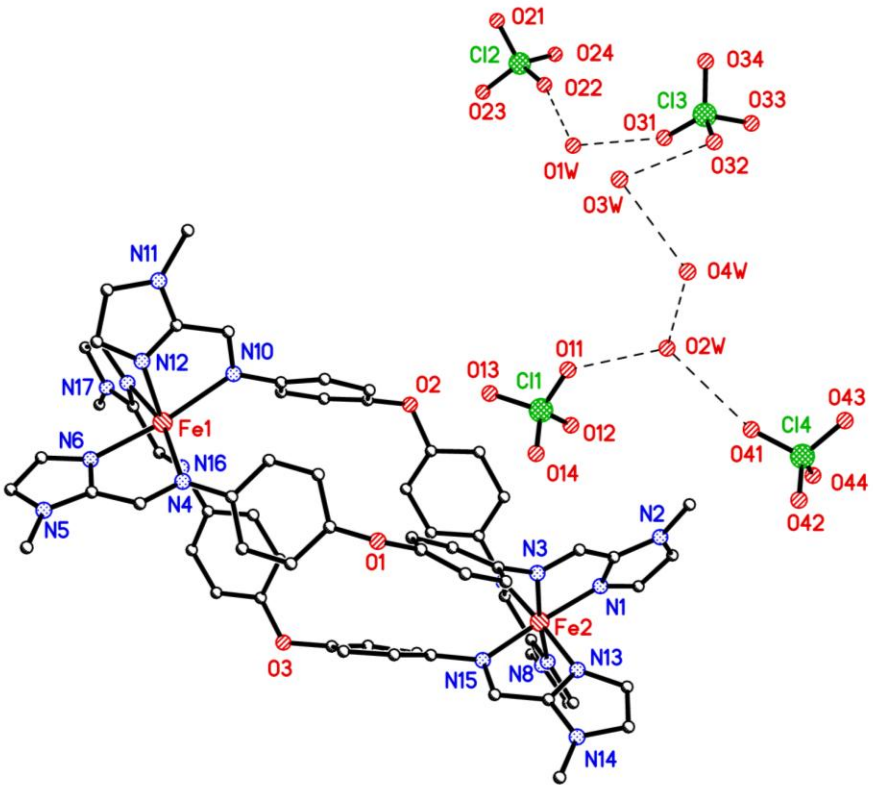

Van't Hoff analysis of susceptibilities for 1.H_2O (typical references 1-3)

A plot was made of ln*K* (y axis) vs 1/*T*

where K = f(HS)/f(LS) = f(HS)/{1-f(HS)} and f (HS) = fraction of high-spin

f(HS) = [($\chi_M T$) - ($\chi_M T$ (LS)]/[$\chi_M T$ (HS) - ($\chi_M T$ (LS)]

The van't Hoff equation is: $d(\ln K)/dT = (\Delta H)/RT^2$

where R is the gas constant (8.314 J mol^{-1} K^{-1}) and ΔH is the total enthalpy change for the spin crossover equilibrium in eqn (1):

$$[Fe(LS)Fe(HS)]^{4+} \overset{K}{\leftrightarrow} [Fe(HS)Fe(HS)]^{4+} \qquad \mathbf{(1)}$$

where $\chi_M T$ (LS) = 0.0624 cm^3 mol^{-1} K, per $2Fe^{II}$, that allows for the 2nd order Zeeman contribution for t_{2g}^6. $\chi_M T$ (HS) is taken from Fig. 3. *NB* $\mu_{eff}^2 = 7.999(\chi_M T)^{0.5}$ from which $\chi_M T$ is any point at temperature T (in Kelvin)

To obtain the entropy change during the spin transition;

$\ln K = - \Delta H/RT + \Delta S/R$

Thus the slope from the linear plot of ln*K* vs 1/*T* , for a gradual spin transition, is $- \Delta H/R$ and the intercept is $\Delta S/R$.

1. R. Boča, M. Boča, H. Ehrenberg, H. Fuess, W. Linert, F. Renz and I. Svoboda, *Chem. Phys.* 2003, **293**, 375-395.
2. T. Nakomoto, Z.- C. Tang and M. Sorai, *Inorg. Chem.* 2001, **40**, 3805-3809.
3. C. M. Grunert, J. Schweifer, P. Weinberger, W. Linert, K. Mereiter, G. Hilscher, M. Müller, G. Weisinger, P. J. Van Koningsbruggen, *Inorg. Chem.* 2004, **43**, 155-165.

Results

Data used for van't Hoff fits, shown below:

1st run is warming 5 K to 300 K; labelled in Fig. 3 as 1st cycle, warming, open circles

2nd run is cooling 300 K to 200 K; labelled in Fig. 3 as 2nd cycle, cooling, filled red circles

3rd run is warming 200 K to 300 K; labelled in Fig. 3 as 2nd cycle, warming, filled red circles

4th run is warming 150 K to 300 K; labelled in Fig. 3 as 3rd cycle, warming, filled red circles

5th run is cooling 300 K to 150 K; labelled in Fig. 3 as 3rd cycle, cooling, filled red circles

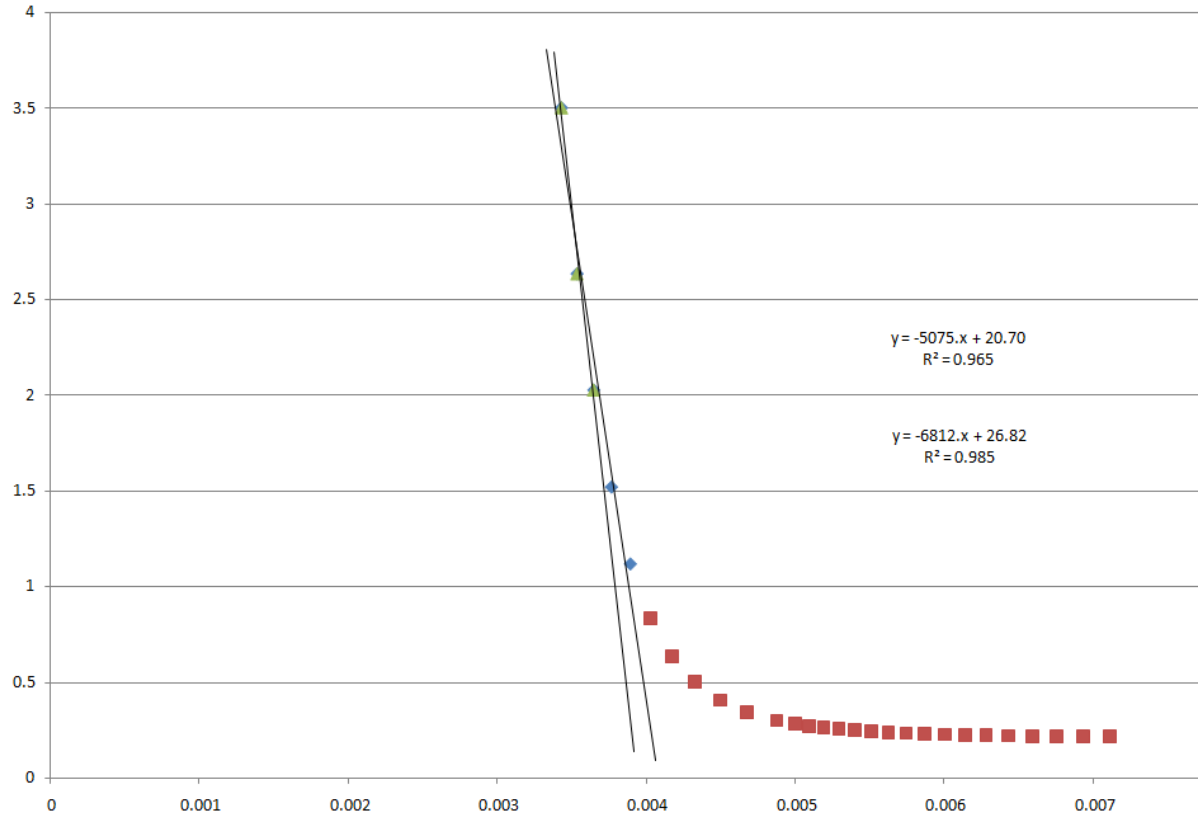

Fig. S6 Van't Hoff plot of ln*K* (y axis) vs. 1/*T* (1/Kelvin) for 1st run of **1.**H_2O. The red squares are the 'half' crossover LS-HS points of Fig. 3. Two linear fits are shown as solid lines giving variations in - $\Delta H/R$ and $\Delta S/R$.

Note that from Fig. 3 it can be seen that run 1 (1st cycle) does not fully reach the HS-HS susceptibility values at 300 K ($1/T$ = 0.0033)

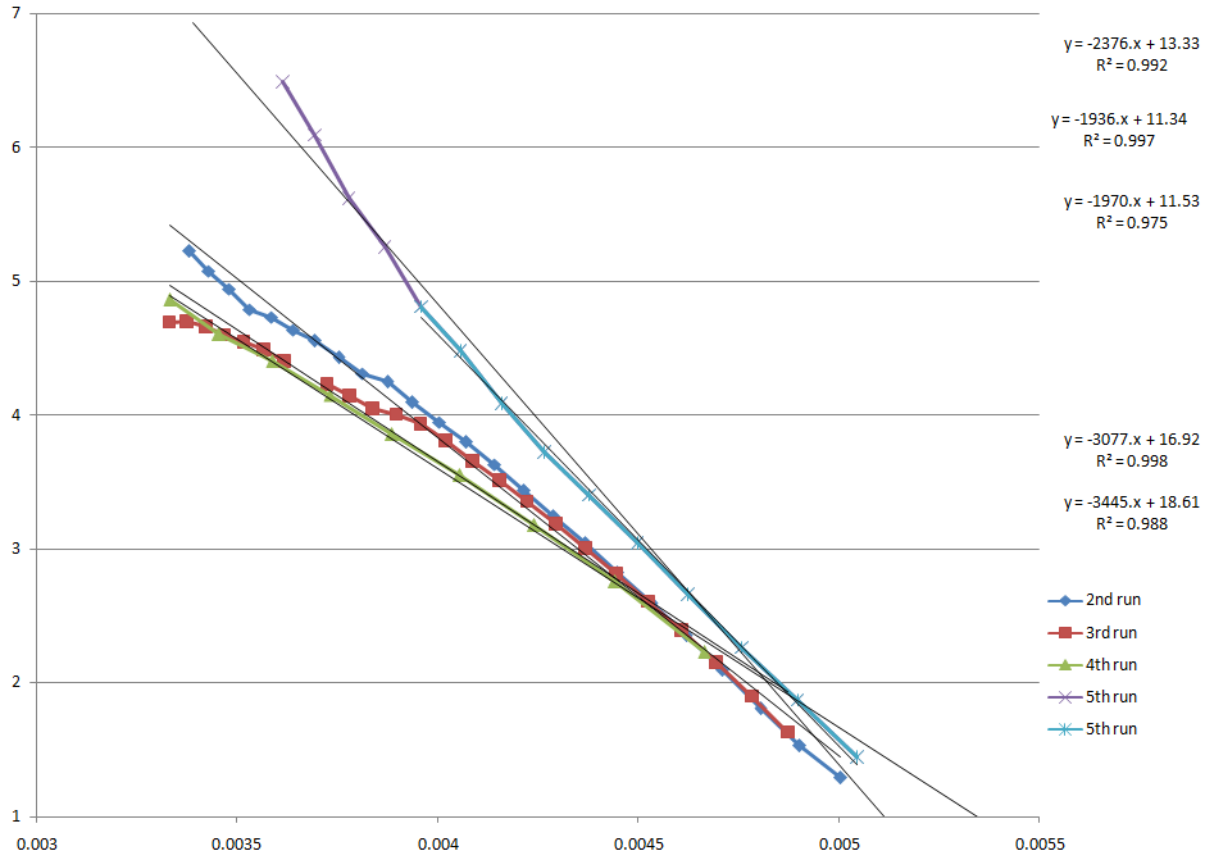

Fig. S7 Van't Hoff plots, and fits to linear eqn, of 2nd, 3rd, 4th (~desolvated forms) and 5th (resolvated) runs for **1** (see relations to Fig 3 caption above). y axis ln*K;* x axis 1/*T* (1/Kelvin).

Fitted values:

1st run (~pristine **1**.H_2O): ΔH = 49(10) kJ mol^{-1} ΔS = 200(30) J mol^{-1} K^{-1}

2nd, 3rd and 4th runs (~desolvated forms): ΔH = 17(2) kJ mol^{-1} ΔS = 100(9) J mol^{-1} K^{-1}

5th run (~resolvated form): ΔH = 27(2) kJ mol^{-1} ΔS = 148(10) J mol^{-1} K^{-1}